Space-time variability of polar cap patches: Direct evidence for internal plasma structuring

H. Dahlgren,[1] G. W. Perry,[2] J. L. Semeter,[1] J.-P. St.-Maurice,[2] K. Hosokawa,[3] M. J. Nicolls,[4] M. Greffen,[5] K. Shiokawa,[6] and C. Heinselman[4]

Received 17 May 2012; revised 6 July 2012; accepted 23 July 2012; published 19 September 2012.

[1] Coordinated observations of ionospheric variability near the geomagnetic pole using the Resolute Bay Incoherent Scatter Radar (RISR-N), Super Dual Auroral Radar Network (SuperDARN) High Frequency (HF) radars, and all-sky imagers have clarified the relative contribution of structuring mechanisms operating on polar plasma patches. From the multipoint RISR-N observations, a three dimensional image can be constructed of the plasma parameters. The colocated coherent echoes from the SuperDARN radars provide information on field aligned irregularities, and from all-sky imagers located in Resolute Bay, Canada and Qaanaaq, Greenland, information is obtained on the emission brightness at different wavelengths. A good correlation is found between the location of the coherent, incoherent and optical signals of patches. From the SuperDARN radar data it is evident that plasma irregularities seem to be present throughout the region of enhanced electron density. The patches are observed to be formed in the cusp region due to bursty flux transfer events and are then transported across the polar cap. During the time period of about 10 minutes when a patch drifted through the RISR-N field of view, the patch seemed to undergo significant deformation in all three spatial dimensions, with density fluctuations of about 10% and spatial variations leading to stretching and tilting of the patch. The findings show that plasma structuring can likely occur within polar cap patches, which support previous suggestions that a patch is highly variable as it drifts across the polar cap, with a faster spread of irregularities throughout the patch as a result.

Citation: Dahlgren, H., G. W. Perry, J. L. Semeter, J.-P. St.-Maurice, K. Hosokawa, M. J. Nicolls, M. Greffen, K. Shiokawa, and C. Heinselman (2012), Space-time variability of polar cap patches: Direct evidence for internal plasma structuring, *J. Geophys. Res.*, *117*, A09312, doi:10.1029/2012JA017961.

1. Introduction

[2] At high-latitudes and over the polar cap, discretized volumes of F-region plasma known as polar cap patches are pushed from the dayside to the nightside ionosphere by convection streams formed by the interaction of the geomagnetic and Interplanetary Magnetic Field (IMF). To be defined as polar cap patches, the volumes of plasma must have a density that is at least twice that of the background F region, and spatial dimensions on the order of 100 km [*Crowley*, 1996]. It is evident that patches are an important mechanism of horizontal plasma transport in the high-latitude and polar cap ionosphere. Observations by *Semeter et al.* [2003] suggest that patches may also play a large role in vertical plasma transport within these regions. Patches are observed under all geomagnetic conditions [e.g., *Coley and Heelis*, 1998] and can be studied optically [e.g., *Buchau et al.*, 1983; *Weber et al.*, 1984; *McEwen and Harris*, 1996; *Moen et al.*, 2002; *Lorentzen et al.*, 2004; *Lockwood et al.*, 2005; *Hosokawa et al.*, 2009a; *Oksavik et al.*, 2010; *Zhang et al.*, 2011] and with radars [e.g., *Rodger et al.*, 1994a; *Pedersen et al.*, 1998; *Carlson et al.*, 2002]. Their effects on radio wave propagation and GPS signals can be significant, even during periods of subdued geomagnetic activity.

[3] Polar cap patches are often detected by their emission of the oxygen emission line at 630.0 nm – the "red line", originating from the $O(^1D)$ state. This state can be reached in many ways, including

$$O_2^+ + e \rightarrow O + O(^1D) \quad (1)$$

$$e^* + O(^3P) \rightarrow e + O(^1D) \quad (2)$$

[1]Department of Electrical and Computer Engineering, Boston University, Boston, Massachusetts, USA.
[2]Institute of Space and Atmospheric Studies, Department of Physics and Engineering Physics, University of Saskatchewan, Saskatoon, Saskatchewan, Canada.
[3]Department of Communication Engineering and Informatics, University of Electro-Communications, Chofu, Japan.
[4]SRI International, Menlo Park, California, USA.
[5]Department of Physics and Astronomy, University of Calgary, Calgary, Canada.
[6]Solar-Terrestrial Environment Laboratory, Nagoya University, Nagoya, Japan.

Corresponding author: H. Dahlgren, Department of Electrical and Computer Engineering, Boston University, 725 Commonwealth Ave., Boston, MA 02215, USA. (hannad@bu.edu)

0148-0227/12/2012JA017961

[e.g., *Garner et al.*, 1996] where e* represents both thermal and photoelectrons. The most important mechanism for generating the red line emissions from polar cap patches is the dissociative recombination shown in equation (1), for which the reaction rate is proportional to the densities of O^+ and O_2 [*Link and Cogger*, 1988].

[4] Depending on its overall size and density, the amount of time for a patch to deplete to a density below that which defines a patch has been estimated to on the order of an hour [*Pedersen et al.*, 1998]. This relatively lengthy lifetime combined with the ability to observe patches with the red-line emission allows for patches to be used as tracers as they drift along E × B convection streams over large geographic areas. Even though the definition of a patch relates to the electron density enhancement above the background, the word patch has generally been used for the regions of red line emission detected in the polar cap by all-sky imagers. Since the image is a two-dimensional projection of an emission dependent on the chemical composition in the ionosphere, there can be a discrepancy between a patch seen by an ISR (Incoherent Scatter Radar) measuring the electron density, and a patch seen by an all-sky imager measuring the red line emission. We will still refer to the optical enhancements discussed in this study as patches, even though their true definition as a patch will be determined by the radar data.

[5] Historically, optical imager experiments have been a popular method for patch observations. Due to their large plasma density gradients and speed, patches are subject to the gradient drift instability (GDI) [*Chaturvedi and Ossakow*, 1981; *Moen et al.*, 2002, 2012]. The irregularities produced from the GDI may set-up a Bragg scattering condition, allowing the patches to be detected outside of the optical spectrum, at radio frequencies, by coherent scatter radar systems [e.g., *Rodger et al.*, 1994a; *Milan et al.*, 2002; *Carlson et al.*, 2002, 2004; *Lockwood et al.*, 2005; *Zhang et al.*, 2011; *Hosokawa et al.*, 2010]. Incoherent scatter radar systems [*Moen et al.*, 2006; *Smith et al.*, 2000], ionosondes [*MacDougall and Jayachandran*, 2007], riometers [*Nishino et al.*, 1998] and rocket-borne instruments [*Lorentzen et al.*, 2010] have all contributed to patch research as well. The majority of early patch research only features data from individual instruments; the infrastructure that would enable patch investigations with more than one instrument had not yet been constructed. To test the self-consistency of our understanding about dynamic processes at work within and around patches, multi-instrument observations are crucial. Recently, the scientific community has placed more emphasis on the high-latitude and polar cap region, investing in new scientific instrumentation there. Within the last decade, the installation of several all-sky imagers at Resolute Bay, like the Optical Mesosphere Thermosphere Imagers (OMTI) [e.g., *Shiokawa et al.*, 1999], two Super Dual Auroral Radar Network (SuperDARN) sites at Rankin Inlet and Inuvik [*Greenwald et al.*, 1995] and the installation of the Resolute Incoherent Scatter Radar - North (RISR-N) at Resolute Bay [*Bahcivan et al.*, 2010], has increased the opportunity to conduct patch research using a variety of complementary instruments. In the near future, the soon to be completed RISR-Canada (RISR-C) ISR will also be able to contribute to patch research, along with a new SuperDARN site at Clyde River – scheduled for construction in summer, 2012.

[6] Multi-instrument observations of polar cap patches have been carried out by for example *Carlson et al.* [2004, 2006]. In the patch case-study by *Lorentzen et al.* [2010] observations from a meridian scanning photometer (MSP), rocket-borne instrumentation and the European Incoherent Scatter (EISCAT) Svalbard Radar (ESR), as well as derived ionospheric convection patterns from the SuperDARN radars were featured. The use of multiple instruments in that study culminated in a significant contribution to patch research: compelling evidence of a strong link between fast convection flows on the edges of a Poleward Moving Auroral Form (PMAF) near the cusp region, and the formation of polar cap patches. The PMAF was observed optically with the MSP, the ESR and rocket were used to measure the plasma density of the PMAF, and the SuperDARN radar was used to infer plasma flows in and around the PMAF and patches. It is important to note that each of the instruments used in this work offered unique and complementary measurements.

[7] Some studies have shown that radar echoes are often stronger on the trailing edge of a patch, attributing this to the notion that GDI growth conditions are more favorable there [*Milan et al.*, 2002; *Cerisier et al.*, 1985]. Observations of multiple patches made both optically and with the Rankin Inlet SuperDARN data by *Hosokawa et al.* [2009b], found no evidence to support this. The radar echoes corresponded well with the optical emissions, even though the lifetime of the patch was shorter than the time needed for the GDI to spread through the patch. A process to account for this discrepancy was presented by *Carlson et al.* [2008], who argued that shear-driven instabilities could rapidly structure the patch during its formation, which was also supported by their measurements.

[8] The complexity and dynamic properties of polar cap patches necessitate a systematic approach for their investigation. Previous work gives credence to the value of using multiple instruments for patch studies. However, each instrument is often limited to measurements in one or two dimensions. In the work presented here, we continue to develop the multi-instrument approach by combining patch measurements from an ISR, a coherent scatter radar and optical instruments. The fast beam-steering technique of the phased-array RISR-N provides a novel three-dimensional view of the plasma parameters in a polar cap patch. This technique was demonstrated on a polar cap patch by *Dahlgren et al.* [2012], who discussed that multiple time-dependent mechanisms can lie behind the high degree of structuring seen in the electron density of the patch. In this paper, we expand on those results, by further investigating the same event, with more depth and a more extensive suite of instrumentation. Reminiscent of the combined observations by *Hosokawa et al.* [2009b] of a patch with SuperDARN and an all-sky imager, where a good correlation between the HF echoes and the optical response was found, we use the RISR-N radar to obtain data on the actual electron density in the polar cap, to compare with SuperDARN echoes, and optical images. The advantages of direct electron density measurements for polar cap studies are many. Instead of projecting line-of-sight integrated optical emissions onto a two-dimensional plane, which does not always reflect the true location of the denser plasma, a three-

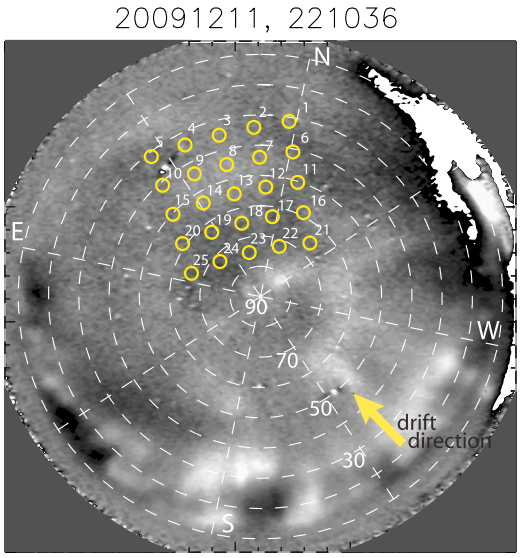

Figure 1. OMTI 630.0 nm image on 11 December 2009, at 22:10 UT. The overplotted small rings show the pointing directions of the 5 × 5 RISR-N beam grid. White dashed lines mark the geographical cardinal directions and elevation angles. The arrow in the bottom right corner shows the general drift direction of the patches from their formation region and through the zenith at Resolute Bay.

dimensional distribution of the electron density can be obtained. The observations are also not weather-dependent. Previous probing of the plasma properties in the polar cap by ISRs have been conducted by the EISCAT Svalbard Radar and the Sondrestrom radar, during slow azimuth or elevation scans [e.g., *Carlson et al.*, 2002; *Valladares et al.*, 1998]. With the capabilities of the RISR-N radar, the probing is no longer limited to two dimensions, and data can be captured simultaneously from all beam directions.

[9] At 22:10 UT on December 11, 2009, a patch was observed for approximately 10 minutes with both the OMTI and RISR-N instruments. At the same time, and in the same region, radar echoes consistent with a patch were detected by both the SuperDARN sites at Rankin Inlet and Saskatoon. The combined data sets allowed for detailed investigation of the ionospheric properties of the patch, and a high degree of intrinsic structuring and variability was indicated in the patch, suggesting that the patch was subject to an internal redistribution of plasma during its transit across the polar cap.

2. Instrumentation and Analysis Techniques

[10] The instrumentation used in this study consists of incoherent and coherent scatter radars and all-sky imagers, which are detailed below:

2.1. RISR-N

[11] The northward-looking Resolute Bay Incoherent Scatter Radar, RISR-N, located in Resolute Bay, Canada (74.7°N, 265.1°E, 83.6°N MLAT), is a modulated phased array radar operated at 449 MHz. Utilizing a beam-steering technique, the pointing direction of the radar can be changed on a pulse-to-pulse basis, providing simultaneous measurements of the polar cap ionosphere in multiple directions when integrating the data over seconds or more. For the data in this study a 480 μs long pulse experiment was run, limiting the line-of-sight range resolution to 72 km. The radar was pointed in a 5 × 5 beam grid, with a beam separation of 14° on average, corresponding to a coverage of about 300 × 400 km at an altitude of 300 km. The pointing directions of the beams are illustrated in Figure 1, as small rings overplotted on one of the OI 630.0 nm OMTI images during the time of the event discussed further below. The geographic cardinal directions as well as the radar beam elevation angle are marked by white dashed lines in the figure. By using a trilinear interpolation technique of the data (illustrated in *Dahlgren et al.* [2012]), based on the techniques described in *Nicolls et al.* [2007] and *Semeter et al.* [2009], a volumetric image of the plasma parameters is obtained at 1 minute resolution.

2.2. SuperDARN Data

[12] The HF SuperDARN radars [*Greenwald et al.*, 1995; *Chisham et al.*, 2007] at Rankin Inlet (62.8°N, 287.0°E), Prince George (54.0°N, 237.4°E), Saskatoon (52.2°N, 253.5°E) and Inuvik (68.4°N, 226.5°E) monitor coherent backscatter from the northern polar cap. SuperDARN radars operate between 8 and 20 MHz. For the times from which the radar data was used, the Rankin Inlet radar was operating at 12.2 MHz, the Prince George radar at 10.7 MHz, the Saskatoon radar at 10.8 MHz and the Inuvik radar at 10.5 MHz. Each SuperDARN radar is capable of electronic beam-steering over an azimuth of approximately 55° that is divided into 16 beams. Each beam is subdivided radially into 100 range gates with a radial resolution of 45 km. These SuperDARN radar field-of-views (FOVs) encompass Resolute Bay, providing backscatter power and line-of-sight velocity estimates with a temporal resolution of 2 min. The FOVs of the four SuperDARN radars are outlined in black in Figure 2, with Rankin Inlet in the center (data colored with gray scale), Saskatoon to the top left (green scale), Prince George to the top center (blue scale) and Inuvik to the top right (red scale).The RISR-N FOV at 270 km altitude is outlined with a red tetragon. The Prince George radar also monitors a region encompassing the cusp during the event discussed here.

2.3. Airglow Imagers

[13] One of the OMTI airglow all-sky imagers is located in Resolute Bay. The imager was developed by the Solar-Terrestrial Environment Laboratory, Nagoya University [*Shiokawa et al.*, 1999; *Hosokawa et al.*, 2006; *Shiokawa et al.*, 2009], and captures a 30 s exposure in 630.0 nm every 2 min and regularly 30 s exposures in 557.7 nm. The 630.0 nm red channel is background corrected, by subtracting a one-hour running average for increased contrast. Due to gaps in the imaging sequence, a similar correction cannot be made for the green 557.7 nm channel. Additional 3 s exposures of N_2^+ at 427.8 nm every 30 s were provided by the NASCAM (Narrow-band All-Sky Camera for Auroral Monitoring) imager owned by the University of Calgary and installed in Resolute Bay.

[14] Data from an all-sky imager installed in Qaanaaq, Greenland (77.5°N, 290.8°E, 85.1°N MLAT) operated by

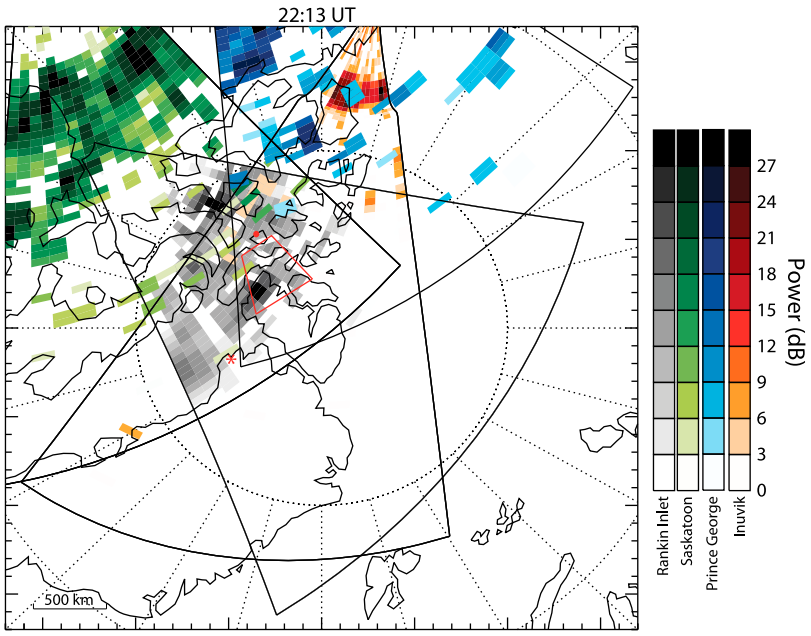

Figure 2. Backscatter power echo fan plot from the SuperDARN radars at Rankin Inlet (gray scale, in center), Saskatoon (green scale, top left), Prince George (blue scale, top center) and Inuvik (red scale, top right), at 22:13 UT. The full FOV of the radars are indicated by black lines. The red tetragon marks the FOV of RISR-N data at 270 km altitude. The patch of particular interest is seen here with the Rankin Inlet radar, within the FOV of RISR-N. Resolute Bay and Qaanaaq are indicated by a red dot and star, respectively. The direction of the Sun is up in the figure.

the U.S. Air Force Research Laboratory are also available for this study. The imager captures 55 s exposures in the red line, at 630.0 nm. The FOV is partly overlapping with the FOV of the OMTI and NASCAM imagers, so that it is possible to continue monitoring the patches as they move out of the range of OMTI.

3. Observations

[15] The polar cap density enhancements discussed in this paper were observed on 11 December 2009, during a very quiet (Kp = 0) period of negative IMF B_z, and negative and positive IMF B_y and B_x, respectively. Faint plasma structures which drifted anti-sunward from their formation region into the polar cap were seen during a time period of a couple of hours following 18 UT. A snapshot of the structures at 630.0 nm taken with the OMTI imager at 22:10:36 UT is shown in Figure 1. The patches come into the FOV from the bottom right corner (geographic south-west) and then drift anti-sunward across the FOV to the north-east. The general direction of the drift is marked in the image with an arrow.

[16] One of the patches drifted through the RISR-N FOV around 22:13 UT, producing enhanced echoes in both the incoherent and coherent scatter radars. Figure 2 shows the SuperDARN power returns at this time, with data from the Saskatoon, Prince George and Rankin Inlet radar. All three color scales are normalized to 30 dB. A stronger echo (darker region) can be seen in the Rankin Inlet data colocated with the RISR-N FOV. The white regions do not necessarily signify the absence of a radar echo, but are most likely due to problems with the fitting of the measured signal, due to low signal-to-noise ratio. Figure 3 shows the correlation between the electron density as measured by RISR-N in a horizontal slice at 270 km altitude (plotted as colored contours in the figure) and the power echo measured by the Rankin Inlet SuperDARN radar (gray scale) at the same time. An enhancement in red line emission could also be detected in the OMTI data, and the location of the emission is marked in the magnified image by a white dashed oval. In Figure 4, range-time plots for backscatter power, velocity and spectral width, from the Rankin Inlet and Saskatoon SuperDARN radar are given. In the former, a transient backscatter power feature – consistent with a patch – can be seen just after 21:50 UT, drifting in a magnetic poleward direction. A similar feature is coincidentally detected by the Saskatoon radar.

[17] A three-dimensional composite of horizontal and vertical slices from the RISR-N data is displayed in Figure 5 for this patch. The slices at 340 km, 250 km and the vertical slice are produced by extracting cuts of the trilinear interpolation of the radar electron density measurements. The positions of the radar beams are marked on each horizontal slice as black circles. This method of visualization and a discussion of the RISR-N data for this particular event has been previously presented in *Dahlgren et al.* [2012]. The structure has a peak electron density of 1.5×10^{11} m^{-3}, close to 250 km in altitude. The contemporary 630.0 nm OMTI image is mapped to 200 km altitude rather than 250 km, to keep the figure from being cluttered. The emission ratio brightness of signal over average background is given by the horizontal color bar at the bottom of the figure. The optical enhancements correspond to the location of the plasma structures seen in the radar data. The coherent scatter

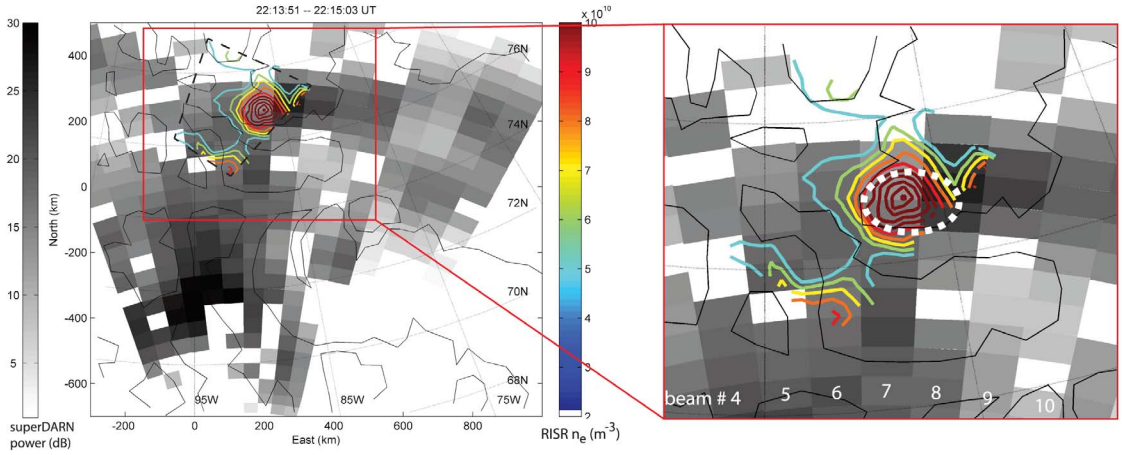

Figure 3. RISR-N electron density contour is plotted in color on top of gray scale SuperDARN echoes. The FOV of RISR-N is outlined by a dashed black line. The coherent scatter in SuperDARN is seen next to the plasma density structure. The white dashed oval in the enlarged figure to the right indicates the location of the optical patch seen with the 630 nm channel on OMTI.

from the SuperDARN radar is then plotted at 300 km altitude. The strongest echo (up to 30 dB, color bar to the left in the figure) comes from the region to the north-east of the vertical slice, partly overlapping the RISR-N plasma structure.

[18] The structure at 22:13 UT is seen in the optical data to arrive from the cusp region (the identification of the cusp will be discussed shortly) and then drift anti-sunward and through the RISR-N FOV at a constant speed. Figure 6 (top)

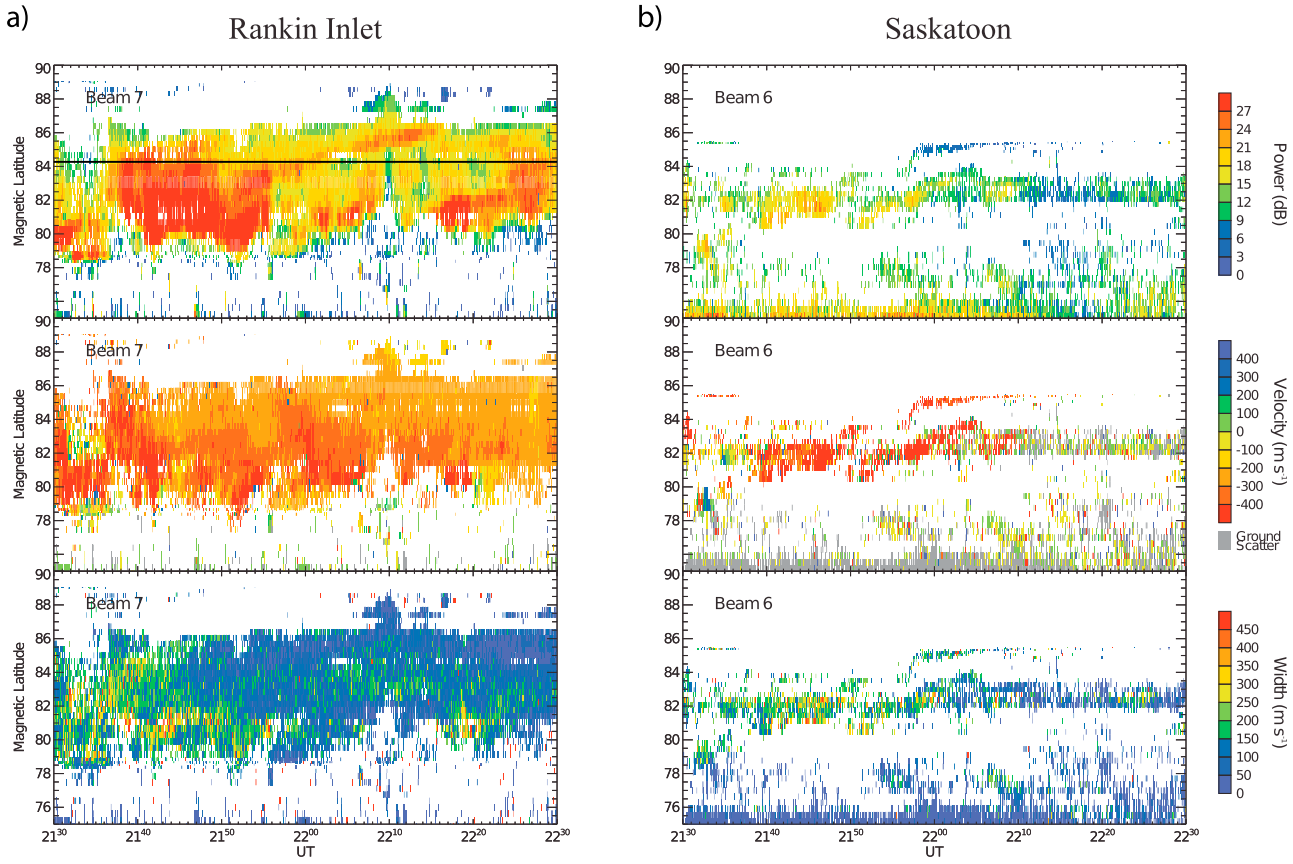

Figure 4. (a) Range-time intensity plot of beam 7 of the SuperDARN radar at Rankin Inlet (top). The latitude of the center of the RISR-N FOV is marked as a black line. (middle) The line-of-sight Doppler velocity and (bottom) the spectral width. (b) Same format as in Figure 4a for data from beam 6 of the Saskatoon radar.

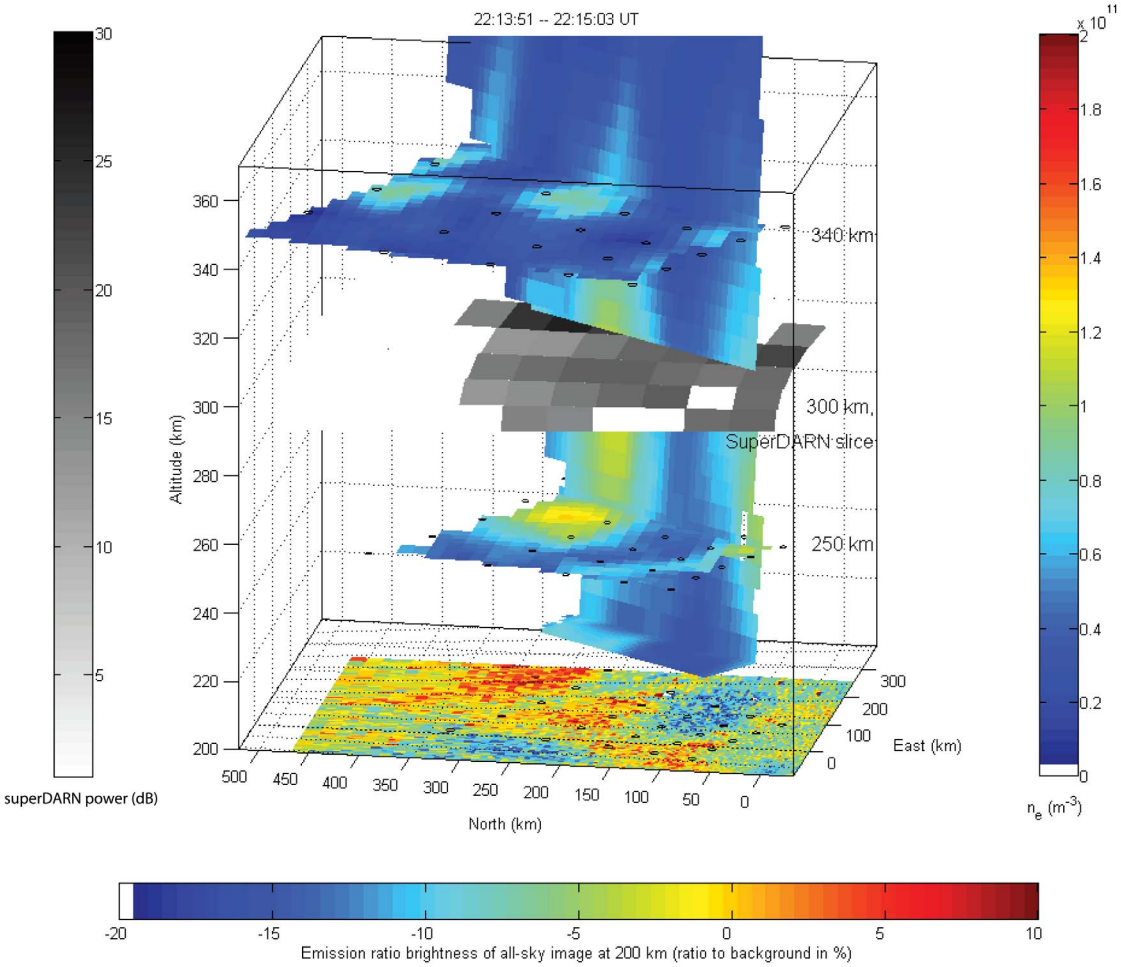

Figure 5. Three-dimensional view of an *F* region plasma density structure. The slices at 350 km and 250 km as well as the vertical slice show the electron density as derived from RISR-N data. The location of the radar beams are marked as black circles on the horizontal slices. At 300 km altitude, the SuperDARN echo is shown. The simultaneous 630.0 nm OMTI image is projected to 200 km altitude, for which the emission brightness over the background level is indicated with the color bar below the combined plot. Optical signatures are seen in the location of plasma density enhancements, whereas the coherent echo from SuperDARN is strongest to the side of the plasma structure.

shows the OMTI meridian-aligned keogram for the time period 22–24 UT, where each slanted structure illustrates a poleward drift. The middle and bottom panels show the derived average velocity and direction of the optical enhancements as they pass the zenith of the OMTI imager. At 22 UT the structures have an optically measured velocity of close to 300 m/s, in the north-east direction. The speed then increases and the direction becomes more eastward. This is consistent with the plasma velocity vectors in the region as constructed from data from the SuperDARN network of HF radars for the same segment of time.

[19] The faint 630.0 nm emissions are also visible in the all-sky data from Qaanaaq, Greenland. At this time, Qaanaaq is located anti-sunward of Resolute Bay and there is some overlap in the FOVs of this imager and the OMTI imager, but unfortunately it was not possible to track a specific patch through both imagers. Even so, red line emission could be seen drifting in the north-east (anti-sunward) direction through the Qaanaaq imager (J. M. Holmes, private communication, 2012).

4. Discussion

[20] In this paper we present simultaneous coherent and volumetric incoherent scatter measurements of polar cap irregularities. The results are compared with optical all-sky measurements in order to clarify the dynamic evolution of polar cap patches, and investigate their intrinsic variability. The weak structures (electron densities of the order of 10^{11} m^{-3}) seen to drift through the RISR-N FOV have spatial sizes of about 100 km × 100 km × 100 km, which is small for typical polar cap patches. Similar horizontal sizes are measured from the optical data. The emissions are also very faint, with brightnesses in the all-sky data of only up to 300 R in 630.0 nm and 50 R in 557.7 nm. The NASCAM imager shows no or very faint emission in the N_2^+ 427.8 nm

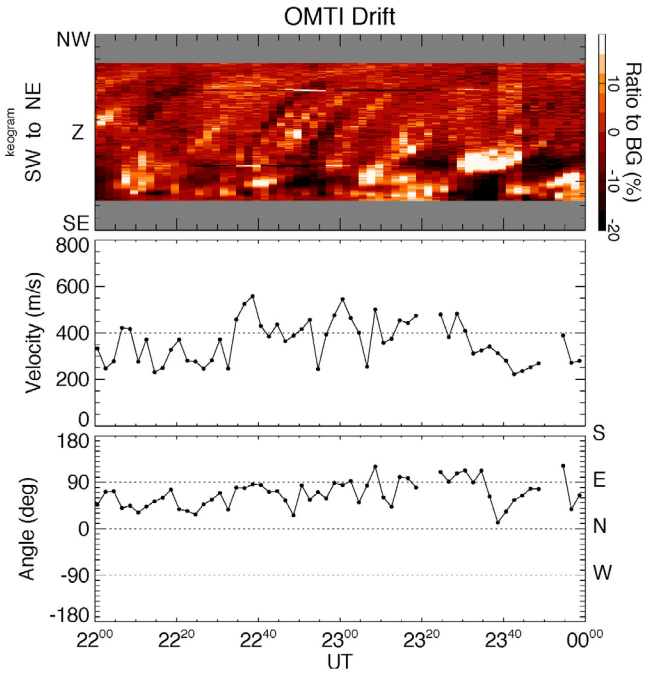

Figure 6. (top) OMTI 630.0 nm keogram along the meridian for the times 22–24 UT. (middle and bottom) The drift velocity of the optical enhancements and their drift angle (east of north), where north is 0 degrees. The structures are drifting predominantly north east, with a velocity of 300–400 m/s.

wavelength region at around 22 UT, which indicates that there is no significant electron precipitation in the polar cap at this time. The structures in the OMTI imager data appear to originate close to the poleward edge of the auroral oval and drift poleward.

4.1. Correlation Between Coherent, Incoherent, and Optical Data

[21] The location of the optical signatures in OMTI correspond well to the enhancements seen in RISR-N for the few hours of contemporary measurements in the two data sets. The coherent backscatter power data from Rankin Inlet SuperDARN radar are indicative of patches in this region during the same time period. In Figure 3, the strongest coherent scatter signal originates from the range gates adjacent to the plasma enhancement seen within the RISR-N FOV. The OMTI all-sky data show a faint optical signature collocated with the RISR-N enhancement at this time. An enlargement of the region of interest is shown in Figure 3, where the location of the optical structure has been marked with a white dashed oval. This comparison shows that the optical structure seen in OMTI overlaps well with the RISR-N structure, and both features straddle two beams (beams 7 and 8) in the SuperDARN FOV, with the strongest echo found in beam 8.

[22] Field aligned irregularities (FAIs) likely produced by the gradient drift instability (GDI) in the plasma set up the Bragg scattering conditions required for coherent backscatter. These FAIs are closely associated with polar cap patches [e.g., *Weber et al.*, 1984; *Rodger et al.*, 1994b; *Ogawa et al.*, 1998; *Hosokawa et al.*, 2009b]. An asymmetry between the irregularity intensity on the leading and trailing edge of a patch is a common feature in patch observations [*Milan et al.*, 2002; *Cerisier et al.*, 1985]. This has been used to infer stronger structuring on the trailing edge and weaker structuring on the leading edge of a patch. The GDI is least stabilized where the E × B velocity of the patch is parallel to the density gradient of the patch, and most stabilized when the E × B velocity of the patch is anti-parallel to the density gradient of the patch. It is therefore expected that the FAI intensity and thus the backscatter power would be higher on the trailing edge of patches [*Cerisier et al.*, 1985]. This explanation for the observed asymmetry was further reinforced by *Milan et al.* [2002], who used the CUTLASS SuperDARN radar in Finland together with an ionosonde located on Svalbard to investigate the structuring of polar cap patches near the cusp. *Hosokawa et al.* [2009b] performed combined SuperDARN radar and all-sky optical measurements on several patches over Resolute Bay. The radar data showed decameter-scale FAIs extending over all of the optically observed polar cap patches, with no preference for the patch edges – contradicting the supposed FAIs preference for the trailing edge of a patch. In their work, *Milan et al.* [2002] and *Ogawa et al.* [1998] speculated that FAI structuring is distributed along the trailing edge of a patch shortly after the formation of the patch. The FAIs then spread over the entire patch during its travel through the polar cap. This was supported by numerical three-dimensional simulations of the nonlinear evolution of instabilities and show that FAI structuring penetrates through the entire patch over a time period of about one hour after its formation [*Gondarenko and Guzdar*, 2004], beginning at the trailing edge of the patch. The patches studied by *Hosokawa et al.* [2009b] were estimated to be only 20–25 min old as they entered the all-sky FOV at Resolute Bay, and were found to be almost fully structured. In other work, in-situ measurements of 18 patches in the polar cap region by the Dynamics Explorer 2 spacecraft showed that the majority of those patches were either fully structured or were structured at the edges, regardless of the distance between the patch and the cusp where they are believed to have formed [*Kivanç and Heelis*, 1997]. Thus there does not appear to be any connection between the spread of FAIs throughout the patch, and the proximity of the patch to the region of its formation. It has also been suggested that auroral particle precipitation in the cusp can give rise to km scale plasma structuring, onto which the GDI can operate [*Kelley et al.*, 1982; *Moen et al.*, 2012]. *Oksavik et al.* [2010] pointed out that polar patches may undergo substantial rotation as they travel, constantly redefining the trailing edge of the patch, increasing the rate at which FAIs occupy the entire patch. In a recent paper by *Carlson et al.* [2008], a possible explanation was offered: a velocity-shear instability may rapidly structure a patch as it is formed, upon which the GDIs then grow. SuperDARN observations were used to support this new mechanism by showing several cases of flow shear in the region where patches were formed. However, no clear evidence of velocity flow shears was detected in the cusp region probed by the Prince George SuperDARN radar during the present event.

[23] The location of the cusp is estimated from the plasma velocity plot in Figure 7 as the region where the drift velocity arrows turn and change from a sunward to an anti-sunward direction, near 75°N MLAT and 12:30 MLT. This location is

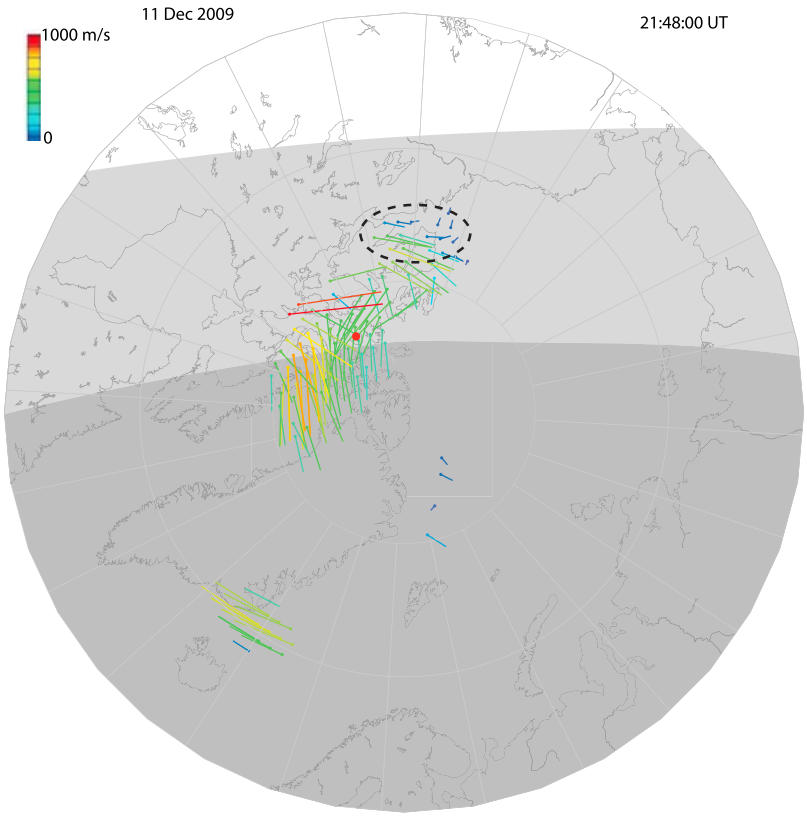

Figure 7. Plasma velocity vectors constructed from line-of-sight velocity information from multiple SuperDARN sites. The plasma flow at Resolute Bay (red dot) is predominantly in the north-east direction. The estimated location of the cusp is marked with a black dashed oval. The transitions to the light and dark gray regions mark the day/night terminators at 300 km altitude and on the ground.

also consistent with modeling for Kp = 0 [*Sigernes et al.*, 2011] and coincident with optical signatures consistent with cusp precipitation and dynamics [e.g., *Milan et al.*, 1999, and references therein]. The distance from Resolute Bay to the cusp is estimated to be 800 km at 22 UT. With an average drift velocity of 300 m/s the patches would be ∼45 min old when they reach the FOV of RISR-N, assuming they were formed in the cusp region. Compared with the patches observed by *Hosokawa et al.* [2009b] we would thus expect the patches in this event to be fully structured by the time they reach Resolute Bay. In Figure 3, the SuperDARN data indicates strong backscatter power throughout the plasma density enhancement observed in the RISR-N data; but the strongest SuperDARN echo is located on the eastern edge of and adjacent to the RISR-N structure. This observation further highlights the indifference of FAIs to align along a leading or trailing edge of patch. It is important to note that the spatial resolution of this SuperDARN data is 45 km radially and ∼50 km azimuthally, with an estimated accuracy of ∼15 km [*Yeoman et al.*, 2001], though the accuracy can be up to 100 km, depending on the HF propagation conditions. Since the RISR-N patch appears to straddle beams 7 and 8 in the SuperDARN FOV, the coherent backscatter echo may have been shifted into an adjacent range gate, creating the appearance of radar echo power in adjacent range gates. A correlation does exist between the SuperDARN echoes in beam 7 and the RISR-N and OMTI signatures; however, their power is less than that of the SuperDARN echoes in beam 8. HF radar backscatter power is not strictly dependent on large density gradients or the amplitude of the FAIs; other effects must be considered. Radio wave propagation conditions play a major role in coherent backscatter. To undergo coherent backscatter, the wave vector of an incident radar beam has to be close to perpendicular (within a few degrees) with the magnetic field in the scattering volume. At high latitudes the magnetic field lines are nearly vertical. In order for the HF radio waves to meet the aspect angle for coherent backscatter, an HF radio wave must undergo refraction, which is possible due to the dispersive properties of ionospheric plasma. The aspect angle condition can be quite sensitive and it is not uncommon to measure a large variation of backscatter power from adjacent range gates or beams, due to propagation conditions. Ray tracing models show that discrete F-region density enhancements (i.e. patches) have similar properties to converging optical lenses causing radio waves incident on the patch to be focused by the patch and then backscatter on the far side of the patch, with respect to the radar. In SuperDARN data this effect would resemble that of Figure 3, in which the strongest backscatter power return in the SuperDARN data is behind the patch in RISR-N and the optical patch in the OMTI data. Therefore, the discrepancy between the locations of the SuperDARN backscatter power and the RISR-N enhancement (Figure 3) may be the result of a combination of the HF propagation conditions and the positioning of the patch between two beams within the SuperDARN FOV.

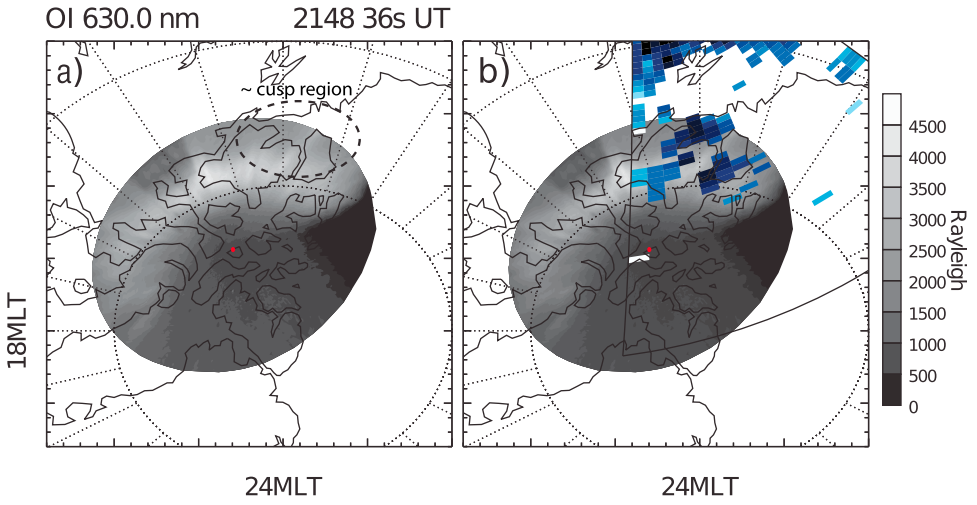

Figure 8. (a) The 630.0 nm OMTI image at 21:48 UT shows the brighter edge corresponding to the formation region of the patches. The red dot marks the location of Resolute Bay and the black dashed oval the estimated location of the cusp. (b) The same OMTI image as in Figure 8a, with the SuperDARN echoes from the radar in Prince George overplotted. Echoes are seen in the region of the cusp, indicative of the strong electrodynamic processes occurring there.

4.2. Formation Mechanism

[24] The substantial amount of instrumentation available for this event is an important asset when characterizing the properties of the polar cap patches, but also in gaining insight into how the structures were formed. Theory suggests that patches may be formed from photoionized plasma originating from subauroral latitudes. The plasma may be transported into the cusp region by convection streamlines and undergo structuring as they reach the cusp [*Foster*, 1993]. The structuring of plasma within the polar cap or cusp region is attributed to a variety of mechanisms such as: transient reconnection and flux transfer events (FTEs) [*Lockwood and Carlson*, 1992], enhanced recombination rates discretizing dense plasma flows, leading to the plasma depletions between the patches [*Valladares et al.*, 1996], and soft particle precipitation creating plasma density enhancements [*Walker et al.*, 1999]. The polar cap itself can be a source of patches; they have been seen to form in the polar cap due to soft precipitation in a region free of photoionization [*Oksavik et al.*, 2006; *Moen et al.*, 2012]. Observations by *Lorentzen et al.* [2010] have also shown that patches may merge from much larger poleward moving auroral forms (PMAFs). In those observations the newly formed patches subsequently convected into the cusp region.

[25] Observations from OMTI in Figure 8a show strong emissions at the 630.0 nm wavelength in the region of the cusp. In the figure, a red dot marks the location of Resolute Bay and the black, dashed oval is roughly the estimated location of the cusp. The SuperDARN radar at Prince George detected an isolated region of backscatter in the same region, which is over-plotted with the OMTI data in Figure 8b. Both of these observations are consistent with previous work investigating HF radar and optical signatures of the cusp and FTEs [*Milan et al.*, 1999; *Moen et al.*, 2001]. In the OMTI data, the position, direction and velocity of the patch was consistent with the convection flow estimates provided by the SuperDARN coverage, as well as the expected ionospheric response to FTEs under IMF $B_y < 0$ conditions [*Milan et al.*, 1999]. Additional observations from NASCAM also show patches emerging from the same region of high optical emissions (the cusp region) first identified in the OMTI data, drifting along the same convection trajectories.

[26] The range time power plot for beam 7 from the Rankin Inlet SuperDARN radar (Figure 4a, top) shows numerous features during a one hour period between 21:30 and 22:30 UT. Magnetic latitude coordinates are provided along the vertical axis and a black horizontal line denotes the magnetic latitude of the center of the RISR-N FOV. A strong echo, identified as the patch of interest from Figure 3, proceeds from a much larger backscatter feature, starting just prior to 22 UT, at ~82°N MLAT. At 22:13 UT, the backscatter power of the patch increases. The same feature is present in the backscatter data measured with the Saskatoon radar, displayed in Figure 4b, but reaches just out of range of this radar at 22:05 UT. The line-of-sight velocity is plotted in the middle panels. The direction of the Doppler velocity is directed away from the radar, with a magnitude of approximately 300 m/s. The velocity features in Figure 4 are consistent with those of pulsed ionospheric flows (PIFs). The poleward moving transient feature in Figure 4 has a velocity that is larger than the surrounding plasma. This is a signature of FTEs [*McWilliams et al.*, 2001; *Provan et al.*, 2002]. The spectral width, a measure of the spread Doppler velocity components within the scattering volume, is plotted in the bottom row of panels in Figure 4. The spectral width of the patch echoes are relatively low, between ~150 and 200 m/s, but seem to have undergone a subtle evolution from a higher spectral width of 250–300 m/s at 79°N MLAT (at about 21:45 UT). The low spectral width and its decrease over time for the patch observed here is again consistent, albeit not as prominent, with the measurements by *McWilliams et al.* [2001] and *Rodger and Rosenberg* [1999], where the spectral width of echoes associated with FTEs evolved from large values, near 400 or 500 m/s, to lower values near 100 to 200 m/s.

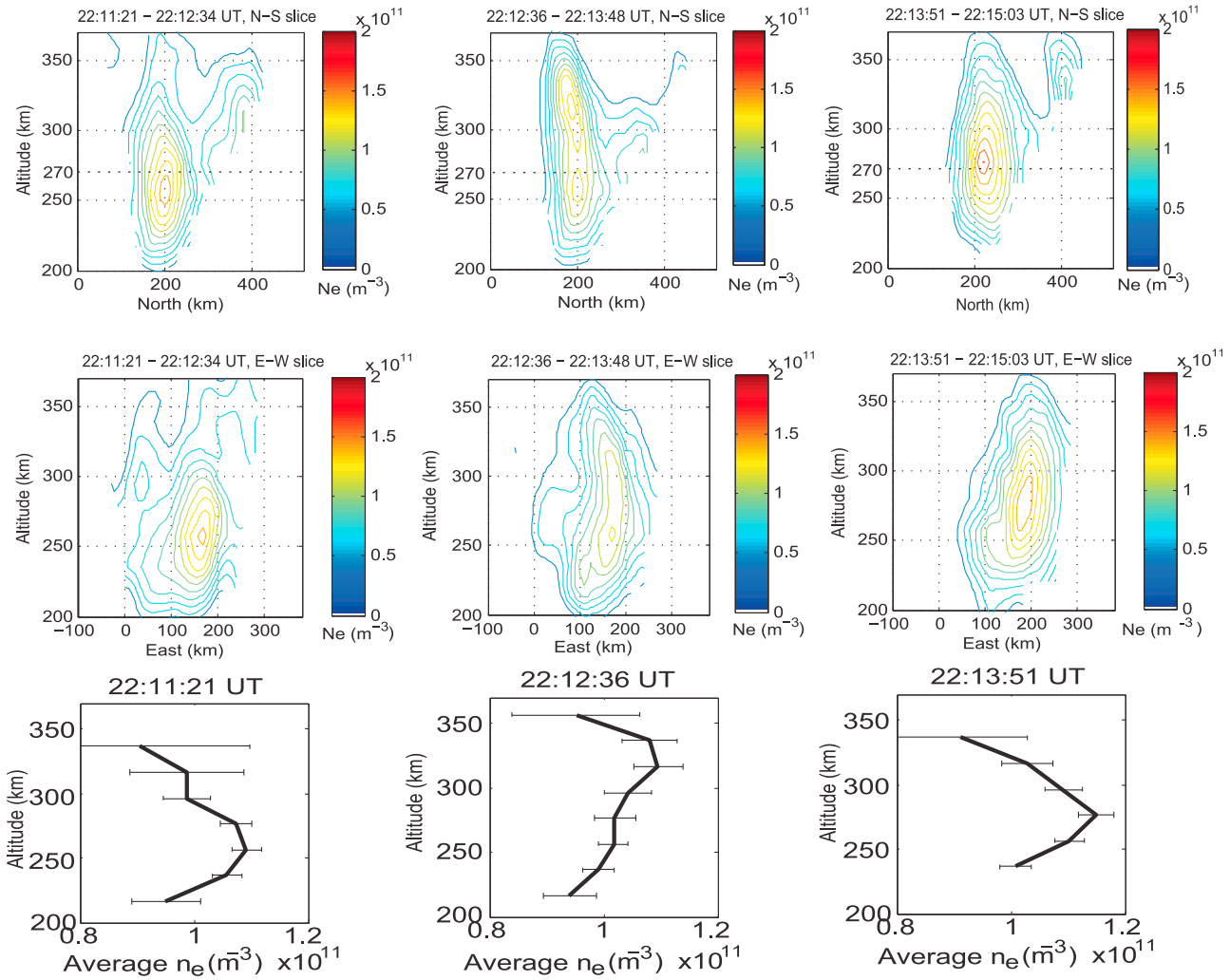

Figure 9. (top) Contour plots of vertical north-south aligned slices through the patch, for the times 22:11:21 UT, 22:12:36 UT and 22:13:51 UT. (middle) Same as top, but for an east-west aligned slice. (bottom) The weighted average vertical density profile of the patch, for each time.

[27] Several other structures are also seen to reach the same latitudes as the patch, north of Resolute Bay, during an interval of a few hours around 22 UT. FTEs between the IMF and the geomagnetic field differ from quasi-stationary reconnection at the dayside magnetopause due to their bursty nature. In the event reported here, bright emission bands are seen in the OMTI optical data to form in the cusp region with 4–8 minute intervals, which then break up to smaller structures as they drift to the north-east with the modeled convection streams. This repetition rate is consistent with the mean period of 8 min found for FTEs in the statistical study by *Rijnbeek et al.* [1984]. The longitudinal motion of the emissions toward the east, observed by OMTI, is also expected during periods of IMF $B_y < 0$ in the northern hemisphere, due to the curvature force on newly opened field lines [*Sandholt et al.*, 1992; *Lockwood et al.*, 1993].

4.3. Investigation of Local Ionization

[28] Figure 9 shows RISR-N data of the temporal evolution of the patch monitored in Figures 3 and 5. In the top row of panels, electron density contours along a vertical north-south directed slice through the center of the patch are displayed for three subsequent time steps. These slices and their horizontal locations were also discussed in *Dahlgren et al.* [2012] (Figure 3). Each slice in Figure 9 is through the center of the patch, and therefore moves with the patch. The northward drift component of the patch is evident in the three time segments. The electron density of the patch is approximately twice that of the background ionosphere. The middle row of panels show the corresponding east-west slice for the same times. The bottom row of panels in Figure 9 show the weighted average of the electron density taken over the whole patch, encompassed by approximately the white dashed circle in Figure 3, as a function of altitude during each of these three time intervals. At 22:11 UT (first column), the electron density peaks close to 260 km altitude. During the next minute of integration the density peak moved up in altitude to 320 km and marginally decreased in magnitude. The data from the subsequent minute (starting at 22:13:51 UT) shows an increased electron density, where the peak altitude dropped to 280 km. The observations are not consistent with patch depletion due to recombination

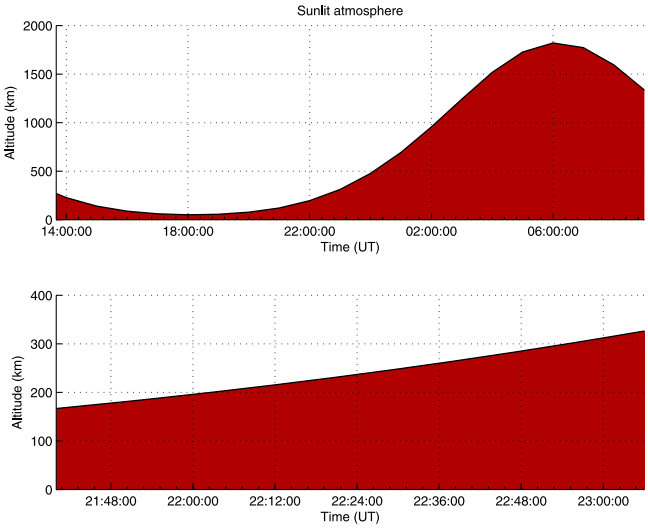

Figure 10. The modeled sunlit atmosphere (white) above Resolute Bay shows that the ionosphere is sunlit above 200 km when the patch drifts through the RISR-N FOV at 22 UT.

with neutrals. The time sequence illustrates a significant variation in the plasma density of the patch over a short period of time. Since the position of the region over which an weighted average of the electron density is being taken (the white dashed line in Figure 3) is moving with the patch, the density variations are not due to the motion of a patch through a stationary reference frame. This is also evident from the bottom row of panels, since they depict the total average density over the whole patch, the variations are not the result of horizontal displacement. The sudden electron density enhancements with a lowering of the peak altitude at 22:13:51 UT suggest that the patch may be experiencing some degree of internal turbulence, resulting in a re-distribution of plasma density, possibly initiated by local precipitation, solar irradiance, or another unknown mechanism.

[29] If soft precipitation is present, an increase in the electron temperature, T_e, would be expected, but the T_e/T_i ratio measured by RISR-N did not show any associated enhancements. The O and N_2^+ emission rates would have increased due to precipitation in the region; however, a close study of the NASCAM imager data associated with these emissions show no significant enhancements indicative of electron precipitation.

[30] The altitude at which the patch event takes place is sunlit at 22:10 UT, which corresponds to 14:25 MLT at Resolute Bay. At this time, the atmosphere is sunlit above 200 km (Figure 10). Photoionization would therefore be underway in the region in and around the patch. The photo production rates of O^+ are significant enough to cause density increase on the order of 10^{11} m^{-3} during the plotted time-segment [*Tohmatsu*, 1990], but the increase would be over a larger region and not as localized as the observed enhancements. Analysis of the density profiles of the ionosphere surrounding the patch do not indicate any significant plasma density changes, consistent with photoionization. The contours suggest a relatively steady plasma density in the vicinity of the patch over a period of a few minutes.

4.4. Interior Plasma Transport

[31] Plasma drift velocities in the horizontal and anti-parallel directions with respect to the background magnetic field can be derived utilizing inversion techniques from the RISR-N line-of-sight ion drift measurements. The horizontal components are split in northward and eastward components and are found to correspond well with the SuperDARN (Figure 7) and OMTI data. From the three dimensional imaging of the patches with RISR-N, we can establish the plasma rest frame in the polar cap ionosphere such that the convection term corresponding to the direction perpendicular to the geomagnetic field, $\nabla_\perp \cdot (n_e \mathbf{u}_{e\perp})$, in the electron continuity equation,

$$\frac{\partial n_e}{\partial t} = P_e - L_e - \frac{\partial}{\partial r}\left(n_e \mathbf{u}_{e\parallel}\right) - \nabla_\perp \cdot (n_e \mathbf{u}_{e\perp}) \tag{3}$$

can be disregarded. The rate of change of the electron density, n_e, of the patch is therefore only governed by ion production (P_e) via impact ionization, chemical loss terms (L_e) and any electron transport along the magnetic field line, $\frac{\partial}{\partial r}\left(n_e \mathbf{u}_{e\parallel}\right)$. The RISR-N data indicates that the patch studied is a closed system with no additional plasma being transported into the region. Despite this, the three profiles in Figure 9 show density variations of around 10% which may be explained by an ionization source between 22:11 UT and 22:13 UT, but none was observed.

[32] The magnitude of the plasma density fluctuations in Figure 9 exceeds the standard deviation, suggesting a redistribution of plasma within the patch. The anti-parallel ion drift obtained from RISR-N data at 84.2°N MLAT, corresponding to the center of the RISR-N FOV and integrated over all altitudes, is displayed in Figure 11. The data suggest that there is little vertical plasma motion in the region, which is further supported by the lack of temperature enhancements due to frictional heating. Upward motion due to neutral winds are also not expected at this latitude, since

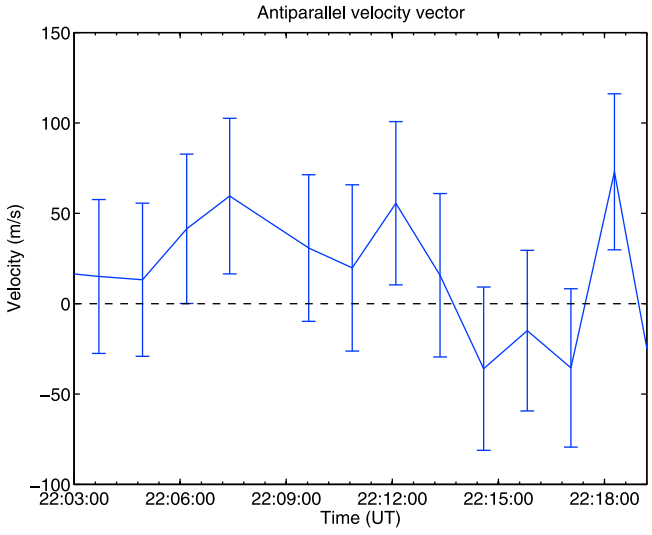

Figure 11. Anti-parallel ion drift velocity, derived from the RISR-N data in the center of the RISR-N FOV. A small increase is seen at 22:12 UT, coincident with an upward shift of the electron density peak in the altitude profiles displayed in Figure 9.

the magnetic field lines are close to vertical. There is a small increase in anti-parallel velocity at 22:12 UT, coinciding with the upward relocation of the electron density peak seen in Figure 9, which then moves to lower altitudes again in the subsequent minute. Nonetheless, it is clear that even the extremum of the velocities measured in Figure 11 can not account for the large density variations seen in Figure 9. This indicates that a large component of the plasma redistribution within the patch may be occurring horizontally. Previous studies [e.g., *Kivanç and Heelis*, 1997; *Hosokawa et al.*, 2009b] have shown that patches are subject to structuring over a range of scale lengths, which may be driven by multiple instabilities [*Basu et al.*, 1990; *Gondarenko and Guzdar*, 2006]. Simulations by *Gondarenko and Guzdar* [2006] illustrate that only a short time is needed for a patch to be fully engulfed with plasma instabilities. In addition, *Carlson et al.* [2008] showed that the irregularities can appear during the formation of the patch, due to shear motion. The observations in Figure 9 may be an example of these instabilities and provide a unique ISR observation of density fluctuations within a patch, due to field-aligned irregularities. Previous observations, specifically those by *Kivanç and Heelis* [1997], were performed by satellite and therefore were unable to provide an unambiguous stationary observation of a patch. However, *Hosokawa et al.* [2010] demonstrated that a polar cap patch can be split into two due to larger scale shear motion in the background convection. The presence of a velocity shear in the patch would indicate the existence of a field-aligned current, which might change the vertical structure of the patch.

[33] The variations of plasma distribution shown in Figure 9 indicate fluctuations within the patch of both intensity as well as spatial distribution of the electron density, with possible velocity shear. A patch is driven by the E × B drift; therefore if E is structured in altitude then the velocity of the patch could be as well. This is assuming that the electric fields within the patch are significant enough to counteract the influence of the large-scale convection electric field. Reports have been made of plasma density fluctuations combined with electric field fluctuations observed by satellites within several patches [*Basu et al.*, 1990; *Kivanç and Heelis*, 1997]. On this note, *Basu et al.* [1990] observed electric field deviations over a range up to ∼30 mV/m – magnitudes on par with the convection electric field. It is however questionable if the presence of intense electric field fluctuations within the patch would be able to produce such large effects as those shown in Figure 9. The optical patches in the OMTI data show no corresponding significant dynamic as they pass the RISR-N FOV. This is to be expected, since the electron density does not change much below 250 km altitude, which is the altitude most of the optical emission originates from. Some variations can be detected in the SuperDARN power, but the changes in the data are not significantly larger than the noise fluctuations.

5. Event on 15 December 2009

[34] The RISR-N 5 × 5 beam experiment was carried out during a few consecutive days in December 2009, during very quiet geophysical conditions. Despite the length of the observations, events with strong electron density enhancements in RISR-N and simultaneously measured echoes in the SuperDARN data from the same region were difficult to find. For this segment of time, most SuperDARN echoes are seen south of Resolute Bay. On 15 December, another event of enhanced electron densities was measured with RISR-N, at around 23 UT. The Kp index at this time was 1, IMF $B_z < 0$, IMF $B_y < 0$, IMF $B_x > 0$ and the plasma features were seen to drift anti-sunward. Figure 12 shows the Rankin Inlet SuperDARN power for three consecutive times in gray scale (with darker regions being stronger echoes). The format is the same as for Figure 3, with the RISR-N electron density contour plot at 300 km altitude superimposed in color on the SuperDARN radar data. A patch of less than 200 km in diameter drifted in from the south into the RISR-N FOV, dispersed and diminished as it reached the center of the FOV. No vertical redistribution of plasma like the one noted for the 11 December event could be seen in this data. At the time of this event, the farmost edge of the SuperDARN scatter reached to halfway through the RISR-N FOV, and larger power is recorded throughout the regions where the patch is seen in the RISR-N electron density data. No specific increase in scatter is seen from the edge of the patch. Larger structures are evident in the radar data from the Rankin Inlet SuperDARN radar, located further south and also drifting anti-sunward at the time. It is possible that these larger patches break up into smaller structures as they drift across the pole [*Hosokawa et al.*, 2010], so that the smaller patch seen by RISR-N is a segment of the larger structure. However, it was not possible to trace the origin of the structure seen in the SuperDARN data.

[35] This event highlights the difficulty in capturing an individual patch with multiple instruments. During this event, the OMTI imager was unusable due to cloud cover over Resolute Bay, leaving only RISR-N and the SuperDARN radars for the observations. Even though RISR-N clearly detected patches, the SuperDARN radars had a more difficult time due to the propagation conditions. Although the event from December 11 demonstrates the validity and usefulness of using multiple instruments to study patches, it should be noted that capturing such a clear event is difficult.

6. Conclusions and Summary

[36] Polar cap patches were observed with incoherent and coherent scatter radars as well as all-sky imagers, as they passed over Resolute Bay. Volumetric imaging of the RISR-N data revealed that the electron density enhancements were largest at around 270 km altitude, with some temporal variations. The low electron densities of $\sim 2 \times 10^{11}$ m^{-3} as well as the height of the patches lead to very faint optical emissions, but it was still possible to trace the patches from their formation region in the cusp, across Resolute Bay and continuing into the FOV of the all-sky imager located further north in Qaanaaq, Greenland. The transient nature of the optical emissions in the formation region and SuperDARN measurements of the patch suggest that the patches may have been formed by the FTE mechanism described by *Lockwood and Carlson* [1992], *Carlson et al.* [2004], *Lockwood et al.* [2005], and *Zhang et al.* [2011]. It is also possible that the internal structuring was initiated by particle precipitation in the cusp [*Kelley et al.*, 1982; *Moen et al.*, 2012]. A more focused study of one of the plasma patches demonstrates a close colocation of the RISR-N, SuperDARN and the all-sky

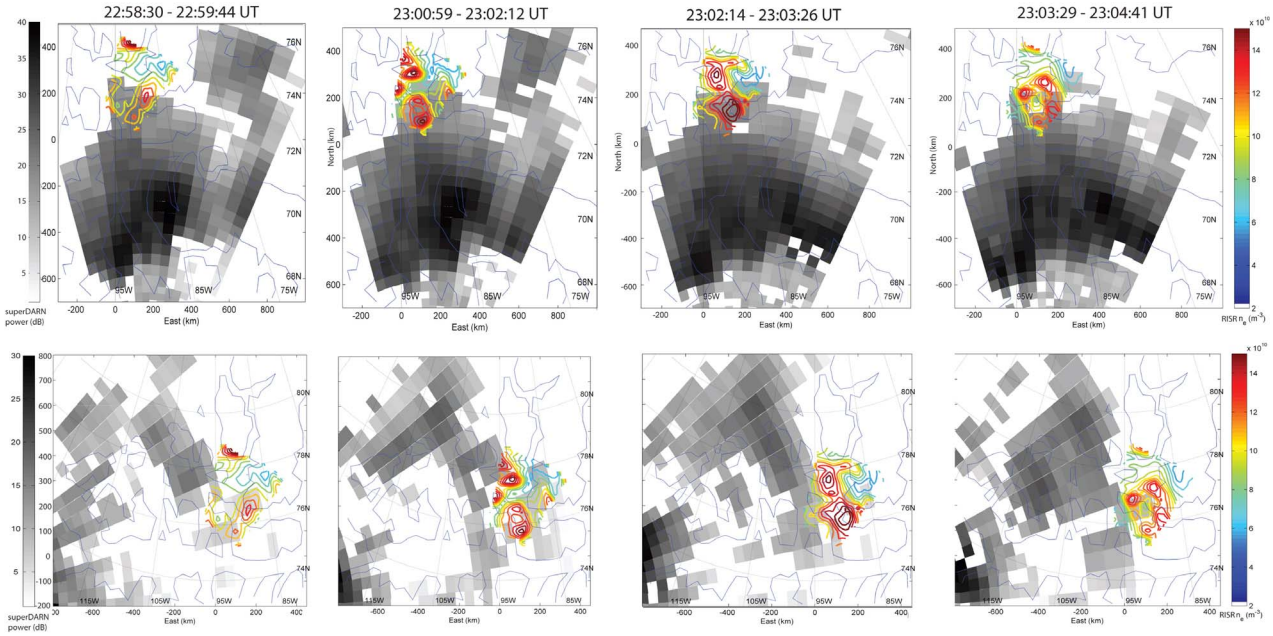

Figure 12. A second polar cap patch was observed in the RISR-N data (colored contour plots) on 15 December 2009, between 22:59 and 23:04 UT. The contemporary SuperDARN echoes are plotted in gray scale, from (top) the Rankin Inlet radar and (bottom) the Inuvik radar. The patch drifts through the RISR-N FOV in the north-east direction and breaks up around 23:04 UT. Although the event is faint, a correlation between the coherent and incoherent scatter data can be discerned. The Rankin Inlet SuperDARN radar also measures strong echoes from large structures south of Resolute Bay (around 70° lat).

data, with the same scale sizes of the regions in all data sets. No evidence of stronger coherent scatter from the trailing edge of the patch is seen, which would be expected for GDI growth on non-rotating, stagnated patches. Instead the irregularities seem to be present throughout the patch, or even strongest on the leading edge. A second event on 15 December 2009 showed a similar correlation, with the measured HF SuperDARN radar scatter taking place throughout the patch. This event is even fainter than the first and the patch is quickly breaking up. Interpretation of the data from these two events should therefore be done with some precaution. Future observations are planned with a specially designed SuperDARN mode with higher spatial resolution over the RISR-N FOV, for a more detailed analysis of similar patches.

[37] From the ISR volumetric data of the individual patch under study, it was indicated that during a short time interval of only a few minutes, significant variations took place, with shape deformations in all spatial directions and velocity shears across the patch. It is noteworthy that these dynamic deformations were observed during a period of Kp = 0. The data indicate that even under these quiet conditions, the patch should not be considered a stagnated feature, but a dynamic and constantly varying structure. This supports the findings by *Oksavik et al.* [2010] who observed rotations of patches during their transit across the polar cap, and suggests that internal motion may also be present, and the patch cannot always be considered a rigid plasma body. It has been learned [*Carlson et al.*, 2008] that irregularity structures in ionospheric patches can be initially driven by the shear instability, not gradient drift, due to strong shears associated with the patch formation process. This leads to structure throughout the patch, a view which our data supports, and establishes the required electron density gradients in the patch to maintain structuring downstream from the high shear formation region. However, our data go beyond this to show that the downstream patch is also actively structured throughout, by dynamics not previously recognized until this work as a further structuring process.

[38] In a novel approach, compared to earlier observations of polar cap patches, optical emissions were not used to first detect the structures; instead the electron density structures measured with the RISR-N radar defined where the patches were located, a method also used in *Dahlgren et al.* [2012]. The patches were then searched for in the SuperDARN and all-sky imager data. The dimness of the patches would have made their initial detection in the all-sky imager data difficult. The faint optical emissions could be mapped to the same geomagnetic latitudinal and longitudinal location as the electron density enhancement, but the altitudes of the two signatures will differ, with the electron density being larger at higher altitudes. This is important to note since patches at higher altitudes will not react with neutrals to produce emissions, and therefore could only be detected with radio instruments. An exception to this is patch detection using 777.4 nm O emissions, since that emission occurs between 250 and 350 km altitude as a result of radiative recombination of O^+ and electrons, and is independent of the neutral atmosphere. The emission was used by *Makela et al.* [2001] for F layer topography maps. However, this emission is also normally very faint which makes it a difficult tracer. The ability to conduct multi-instrument patch experiments

provides the opportunity to gain further insight into the properties and dynamics of patches and is crucial when trying to understand and investigate their formation, evolution and characteristics. In most cases, like the one reported here, a single instrument cannot provide sufficient measurements to investigate the intricacies of a patch.

[39] **Acknowledgments.** The operations and maintenance of RISR-N is supported by National Science Foundation (NSF) cooperative agreement ATM-0608577 to SRI International. The optical measurement at Resolute Bay was supported by Grants-in-Aid for Scientific Research (16403007, 19403010, and 20244080) from the Japan Society for the Promotion of Science (JSPS). This work was partially supported by the U.S. Air Force Office of Scientific Research under contract FA9550-12-1-018. We thank J.M. Holmes for discussions and analysis of the Qaanaaq imager data. This work was initiated by discussions which took place at the Coupling, Energetics and Dynamics of Atmospheric Regions (CEDAR) workshop 2011. HD and GP thank NSF for the CEDAR student support.

[40] Robert Lysak thanks the reviewers for their assistance in evaluating this paper.

References

Bahcivan, H., R. Tsunoda, M. Nicolls, and C. Heinselman (2010), Initial ionospheric observations made by the new Resolute incoherent scatter radar and comparison to solar wind IMF, *Geophys. Res. Lett.*, *37*, L15103, doi:10.1029/2010GL043632.

Basu, S., S. Basu, E. MacKenzie, W. R. Coley, J. R. Sharber, and W. R. Hoegy (1990), Plasma structuring by the gradient drift instability at high latitudes and comparison with velocity shear driven processes, *J. Geophys. Res.*, *95*(A6), 7799–7818, doi:10.1029/JA095iA06p07799.

Buchau, J., B. W. Reinisch, E. J. Weber, and J. G. Moore (1983), Structure and dynamics of the winter polar cap *F* region, *Radio Sci.*, *18*(6), 995–1010, doi:10.1029/RS018i006p00995.

Carlson, H. C., K. Oksavik, J. Moen, A. P. van Eyken, and P. Guio (2002), ESR mapping of polar-cap patches in the dark cusp, *Geophys. Res. Lett.*, *29*(10), 1386, doi:10.1029/2001GL014087.

Carlson, H. C., Jr., K. Oksavik, J. Moen, and T. Pedersen (2004), Ionospheric patch formation: Direct measurements of the origin of a polar cap patch, *Geophys. Res. Lett.*, *31*, L08806, doi:10.1029/2003GL018166.

Carlson, H. C., J. Moen, K. Oksavik, C. P. Nielsen, I. W. McCrea, T. R. Pedersen, and P. Gallop (2006), Direct observations of injection events of subauroral plasma into the polar cap, *Geophys. Res. Lett.*, *33*, L05103, doi:10.1029/2005GL025230.

Carlson, H. C., K. Oksavik, and J. Moen (2008), On a new process for cusp irregularity production, *Ann. Geophys.*, *26*, 2871–2885, doi:10.5194/angeo-2628712008.

Cerisier, J. C., J. J. Berthelier, and C. Beghin (1985), Unstable density gradients in the high-latitude ionosphere, *Radio Sci.*, *20*(4), 755–761, doi:10.1029/RS020i004p00755.

Chaturvedi, P. K., and S. L. Ossakow (1981), The current convective instability as applied to the auroral ionosphere, *J. Geophys. Res.*, *86*(A6), 4811–4814, doi:10.1029/JA086iA06p04811.

Chisham, G., et al. (2007), A decade of the Super Dual Auroral Radar Network (SuperDARN): scientific achievements, new techniques and future directions, *Surv. Geophys.*, *28*, 33–109, doi:10.1007/s1071200790178.

Coley, W. R., and R. A. Heelis (1998), Structure and occurrence of polar ionization patches, *J. Geophys. Res.*, *103*(A2), 2201–2208, doi:10.1029/97JA03345.

Crowley, G. (1996), Critical review of ionospheric patches and blobs, in *Review of Radio Science: 1993–1996*, edited by W. R. Stone, pp. 619–648, Oxford Univ. Press, Oxford, U. K.

Dahlgren, H., J. L. Semeter, K. Hosokawa, M. J. Nicolls, T. W. Butler, M. G. Johnsen, K. Shiokawa, and C. Heinselman (2012), Direct three-dimensional imaging of polar ionospheric structures with the Resolute Bay Incoherent Scatter Radar, *Geophys. Res. Lett.*, *39*, L05104, doi:10.1029/2012GL050895.

Foster, J. C. (1993), Storm time plasma transport at middle and high latitudes, *J. Geophys. Res.*, *98*(A2), 1675–1689, doi:10.1029/92JA02032.

Garner, T. W., T. L. Killeen, A. G. Burns, J. D. Winningham, and W. R. Coley (1996), Examination of the oxygen red line signature of a polar cap ionization patch as seen from the Dynamics Explorer 2 satellite, *Radio Sci.*, *31*(3), 607–618, doi:10.1029/96RS00617.

Gondarenko, N. A., and P. N. Guzdar (2004), Plasma patch structuring by the nonlinear evolution of the gradient drift instability in the high-latitude ionosphere, *J. Geophys. Res.*, *109*, A09301, doi:10.1029/2004JA010504.

Gondarenko, N. A., and P. N. Guzdar (2006), Nonlinear three-dimensional simulations of mesoscale structuring by multiple drives in high-latitude plasma patches, *J. Geophys. Res.*, *111*, A08302, doi:10.1029/2006JA011701.

Greenwald, R. A., et al. (1995), DARN/SuperDARN, *Space Sci. Rev.*, *71*, 761–796, doi:10.1007/BF00751350.

Hosokawa, K., K. Shiokawa, Y. Otsuka, A. Nakajima, T. Ogawa, and J. D. Kelly (2006), Estimating drift velocity of polar cap patches with all-sky airglow imager at Resolute Bay, Canada, *Geophys. Res. Lett.*, *33*, L15111, doi:10.1029/2006GL026916.

Hosokawa, K., T. Kashimoto, S. Suzuki, K. Shiokawa, Y. Otsuka, and T. Ogawa (2009a), Motion of polar cap patches: A statistical study with all-sky airglow imager at Resolute Bay, Canada, *J. Geophys. Res.*, *114*, A04318, doi:10.1029/2008JA014020.

Hosokawa, K., K. Shiokawa, Y. Otsuka, T. Ogawa, J.-P. St-Maurice, G. J. Sofko, and D. A. Andre (2009b), Relationship between polar cap patches and field-aligned irregularities as observed with an all-sky airglow imager at Resolute Bay and the PolarDARN radar at Rankin Inlet, *J. Geophys. Res.*, *114*, A03306, doi:10.1029/2008JA013707.

Hosokawa, K., J.-P. St-Maurice, G. J. Sofko, K. Shiokawa, Y. Otsuka, and T. Ogawa (2010), Reorganization of polar cap patches through shears in the background plasma convection, *J. Geophys. Res.*, *115*, A01303, doi:10.1029/2009JA014599.

Kelley, M. C., J. F. Vickrey, C. W. Carlson, and R. Torbert (1982), On the origin and spatial extent of high-latitude *F* region irregularities, *J. Geophys. Res.*, *87*(A6), 4469–4475, doi:10.1029/JA087iA06p04469.

Kivanç, Ö., and R. A. Heelis (1997), Structures in ionospheric number density and velocity associated with polar cap ionization patches, *J. Geophys. Res.*, *102*, 307–318, doi:10.1029/96JA03141.

Link, R., and L. L. Cogger (1988), A reexamination of the O I 6300-Ånight-glow, *J. Geophys. Res.*, *93*, 9883–9892, doi:10.1029/JA093iA09p09883.

Lockwood, M., and H. C. Carlson Jr. (1992), Production of polar cap electron density patches by transient magnetopause reconnection, *Geophys. Res. Lett.*, *19*(17), 1731–1734, doi:10.1029/92GL01993.

Lockwood, M., H. C. Carlson Jr., and P. E. Sandholt (1993), Implications of the altitude of transient 630-nm dayside auroral emissions, *J. Geophys. Res.*, *98*(A9), 15,571–15,587, doi:10.1029/93JA00811.

Lockwood, M., J. A. Davies, J. Moen, A. P. van Eyken, K. Oksavik, I. W. McCrea, and M. Lester (2005), Motion of the dayside polar cap boundary during substorm cycles: II. Generation of poleward-moving events and polar cap patches by pulses in the magnetopause reconnection rate, *Ann. Geophys.*, *23*, 3513–3532, doi:10.5194/angeo-2335132005.

Lorentzen, D. A., N. Shumilov, and J. Moen (2004), Drifting airglow patches in relation to tail reconnection, *Geophys. Res. Lett.*, *31*, L02806, doi:10.1029/2003GL017785.

Lorentzen, D. A., J. Moen, K. Oksavik, F. Sigernes, Y. Saito, and M. G. Johnsen (2010), In situ measurement of a newly created polar cap patch, *J. Geophys. Res.*, *115*, A12323, doi:10.1029/2010JA015710.

MacDougall, J., and P. T. Jayachandran (2007), Polar patches: Auroral zone precipitation effects, *J. Geophys. Res.*, *112*, A05312, doi:10.1029/2006JA011930.

Makela, J. J., M. C. Kelley, S. A. González, N. Aponte, and R. P. McCoy (2001), Ionospheric topography maps using multiple-wavelength all-sky images, *J. Geophys. Res.*, *106*(A12), 29,161–29,174, doi:10.1029/2000JA000449.

McEwen, D. J., and D. P. Harris (1996), Occurrence patterns of *F* layer patches over the north magnetic pole, *Radio Sci.*, *31*(3), 619–628, doi:10.1029/96RS00312.

McWilliams, K. A., T. K. Yeoman, and S. W. H. Cowley (2001), Two-dimensional electric field measurements in the ionospheric footprint of a flux transfer event, *Ann. Geophys.*, *18*, 1584–1598, doi:10.1007/s0058500115842.

Milan, S. E., M. Lester, S. W. H. Cowley, J. Moen, P. E. Sandholt, and C. J. Owen (1999), Meridian-scanning photometer, coherent HF radar, and magnetometer observations of the cusp: A case study, *Ann. Geophys.*, *17*, 159–172, doi:10.1007/s0058599901595.

Milan, S. E., M. Lester, and T. K. Yeoman (2002), HF radar polar patch formation revisited: Summer and winter variations in dayside plasma structuring, *Ann. Geophys.*, *20*, 487–499.

Moen, J., H. C. Carlson, S. E. Milan, N. Shumilov, B. Lybbekk, P. E. Sandholt, and M. Lester (2001), On the collocation between dayside auroral activity and coherent HF radar backscatter, *Ann. Geophys.*, *18*, 1531–1549, doi:10.1007/s0058500115312.

Moen, J., I. K. Walker, L. Kersley, and S. E. Milan (2002), On the generation of cusp HF backscatter irregularities, *J. Geophys. Res.*, *107*(A4), 1044, doi:10.1029/2001JA000111.

Moen, J., H. C. Carlson, K. Oksavik, C. P. Nielsen, S. E. Pryse, H. R. Middleton, I. W. McCrea, and P. Gallop (2006), EISCAT observations of plasma patches at sub-auroral cusp latitudes, *Ann. Geophys.*, *24*, 2363–2374, doi:10.5194/angeo-2423632006.

Moen, J., K. Oksavik, T. Abe, M. Lester, Y. Saito, T. A. Bekkeng, and K. S. Jacobsen (2012), First in-situ measurements of HF radar echoing targets, *Geophys. Res. Lett.*, *39*, L07104, doi:10.1029/2012GL051407.

Nicolls, M. J., C. J. Heinselman, E. A. Hope, S. Ranjan, M. C. Kelley, and J. D. Kelly (2007), Imaging of polar mesosphere summer echoes with the 450 MHz poker flat advanced modular incoherent scatter radar, *Geophys. Res. Lett.*, *34*, L20102, doi:10.1029/2007GL031476.

Nishino, M., S. Nozawa, and J. Holtet (1998), Daytime ionospheric absorption features in the polar cap associated with poleward drifting *F*-region plasma patches, *Earth Planets Space*, *50*, 107–117.

Ogawa, T., N. Nishitani, M. Pinnock, N. Sato, H. Yamagishi, and A. S. Yukimatu (1998), Antarctic HF radar observations of irregularities associated with polar patches and auroral blobs: A case study, *J. Geophys. Res.*, *103*(A11), 26,547–26,558, doi:10.1029/98JA02044.

Oksavik, K., J. M. Ruohoniemi, R. A. Greenwald, J. B. H. Baker, J. Moen, H. C. Carlson, T. K. Yeoman, and M. Lester (2006), Observations of isolated polar cap patches by the European Incoherent Scatter (EISCAT) Svalbard and Super Dual Auroral Radar Network (SuperDARN) Finland radars, *J. Geophys. Res.*, *111*, A05310, doi:10.1029/2005JA011400.

Oksavik, K., V. L. Barth, J. Moen, and M. Lester (2010), On the entry and transit of high-density plasma across the polar cap, *J. Geophys. Res.*, *115*, A12308, doi:10.1029/2010JA015817.

Pedersen, T. R., B. G. Fejer, R. A. Doe, and E. J. Weber (1998), Incoherent scatter radar observations of horizontal *F* region plasma structure over Sondrestrom, Greenland, during polar cap patch events, *Radio Sci.*, *33*(6), 1847–1866, doi:10.1029/98RS01702.

Provan, G., S. E. Milan, M. Lester, T. K. Yeoman, and H. Khan (2002), Letter to the Editor: Simultaneous observations of the ionospheric footprint of flux transfer events and dispersed ion signatures, *Ann. Geophys.*, *20*, 281–287, doi:10.5194/angeo-202812002.

Rijnbeek, R. P., S. W. H. Cowley, D. J. Southwood, and C. T. Russell (1984), A survey of dayside flux transfer events observed by ISEE 1 and 2 magnetometers, *J. Geophys. Res.*, *89*(A2), 786–800, doi:10.1029/JA089iA02p00786.

Rodger, A. S., M. Pinnock, J. R. Dudeney, J. Waterman, O. de la Beaujardiere, and K. B. Baker (1994a), Simultaneous two hemisphere observations of the presence of polar patches in the nightside ionosphere, *Ann. Geophys.*, *12*, 642–648, doi:10.1007/s005859940642y.

Rodger, A. S., M. Pinnock, J. R. Dudeney, and K. B. Baker (1994b), A new mechanism for polar patch formation, *J. Geophys. Res.*, *99*, 6425–6436, doi:10.1029/93JA01501.

Rodger, A. S., and T. J. Rosenberg (1999), Riometer and HF radar signatures of polar patches, *Radio Sci.*, *34*(2), 501–508, doi:10.1029/1998RS900005.

Sandholt, P. E., M. Lockwood, W. F. Denig, R. C. Elphic, and S. Leont'ev (1992), Dynamical auroral structure in the vicinity of the polar cusp - Multipoint observations during southward and northward IMF, *Ann. Geophys.*, *10*, 483–497.

Semeter, J., C. J. Heinselman, J. P. Thayer, R. A. Doe, and H. U. Frey (2003), Ion upflow enhanced by drifting *F*-region plasma structure along the nightside polar cap boundary, *Geophys. Res. Lett.*, *30*(22), 2139, doi:10.1029/2003GL017747.

Semeter, J., T. Butler, C. Heinselman, M. Nicolls, J. Kelly, and D. Hampton (2009), Volumetric imaging of the auroral ionosphere: Initial results from PFISR, *J. Atmos. Sol. Terr. Phys.*, *71*, 738–743, doi:10.1016/j.jastp.2008.08.014.

Shiokawa, K., Y. Katoh, M. Satoh, M. K. Ejiri, T. Ogawa, T. Nakamura, T. Tsuda, and R. H. Wiens (1999), Development of Optical Mesosphere Thermosphere Imagers (OMTI), *Earth Planets Space*, *51*, 887–896.

Shiokawa, K., Y. Otsuka, and T. Ogawa (2009), Propagation characteristics of nighttime mesospheric and thermospheric waves observed by optical mesosphere thermosphere imagers at middle and low latitudes, *Earth Planets Space*, *61*, 470–491.

Sigernes, F., M. Dyrland, P. Brekke, S. Chernouss, D. A. Lorentzen, K. Oksavik, and C. S. Deehr (2011), Two methods to forecast auroral displays, *J. Space Weather Space Clim.*, *1*, A03, doi:10.1051/swsc/2011003.

Smith, A. M., S. E. Pryse, and L. Kersley (2000), Polar patches observed by ESR and their possible origin in the cusp region, *Ann. Geophys.*, *18*, 1043–1053, doi:10.1007/s0058500010435.

Tohmatsu, T. (1990), *Compendium of Aeronomy*, Terra Sci., Tokyo.

Valladares, C. E., D. T. Decker, R. Sheehan, and D. N. Anderson (1996), Modeling the formation of polar cap patches using large plasma flows, *Radio Sci.*, *31*(3), 573–593, doi:10.1029/96RS00481.

Valladares, C. E., D. T. Decker, R. Sheehan, D. N. Anderson, T. Bullett, and B. W. Reinisch (1998), Formation of polar cap patches associated with north-to-south transitions of the interplanetary magnetic field, *J. Geophys. Res.*, *103*(A7), 14,657–14,670, doi:10.1029/97JA03682.

Walker, I. K., J. Moen, L. Kersley, and D. A. Lorentzen (1999), On the possible role of cusp/cleft precipitation in the formation of polar-cap patches, *Ann. Geophys.*, *17*, 1298–1305, doi:10.1007/s0058599912984.

Weber, E. J., J. Buchau, J. G. Moore, J. R. Sharber, R. C. Livingston, J. D. Winningham, and B. W. Reinisch (1984), *F* layer ionization patches in the polar cap, *J. Geophys. Res.*, *89*(A3), 1683–1694, doi:10.1029/JA089iA03p01683.

Yeoman, T. K., D. M. Wright, A. J. Stocker, and T. B. Jones (2001), An evaluation of range accuracy in the Super Dual Auroral Radar Network over-the-horizon HF radar systems, *Radio Sci.*, *36*, 801–813, doi:10.1029/2000RS002558.

Zhang, Q.-H., et al. (2011), On the importance of interplanetary magnetic field B_y on polar cap patch formation, *J. Geophys. Res.*, *116*, A05308, doi:10.1029/2010JA016287.